

# **Differential state-dependence of low and high firing neurons in the hippocampus**

Hiroyuki Miyawaki, PhD<sup>†</sup>, Kamran Diba, PhD\*

Department of Psychology, University of Wisconsin-Milwaukee, 2441 E Hartford Ave,  
Milwaukee, WI 53211

<sup>†</sup> Present address: Department of Physiology, Graduate School of Medicine, Osaka City  
University, Asahimachi 1-4-3, Abeno-ku, Osaka, 545-8585, Japan

\* Correspondence to: [diba@uwm.edu](mailto:diba@uwm.edu); Tel: 414-229-5740; Fax: 414-229-5219.

This manuscript contains 4 figures, no tables, and 3 supplementary figures.

This work is supported by NIH R01MH109170 to K.D..

The authors disclose that there are no off-label or investigational use, no conflicts of interest, and no clinical trials.

# Abstract

Recent evidence suggests that low and high firing neurons display different plasticity and dynamics. We therefore investigated the effects of sleep and waking states and state transitions on hippocampal CA1 neurons with a log-normal distribution of firing rates. We analyzed single unit spiking from 1017 putative pyramidal cells and 116 putative interneurons along with local field potentials of hippocampal CA1 region recorded in 19 sessions from male rats during natural wake/sleep across the 24-hr cycle. We separated cells into five quantiles based on firing rates, and implemented a shuffle-corrected deflection index to account for changes relative to regression to the mean. Firing-rate changes within non-REM sleep, REM sleep, and state transitions from non-REM to REM favored higher-firing neurons, with either smaller increases or stronger decreases among lower-firing neurons. In contrast, transitions from REM to non-REM sleep reduced variability across population, resulting in higher firing among lower-firing neurons and vice versa. These changes account for previously reported net decrease of firing rate across sleep, with the largest decrease occurring in lower-firing cells, while moderately-firing cells show the greatest firing increases during waking. These results demonstrate that sleep/wake states and state transitions affect lower and higher-firing neurons differently, with non-REM sleep playing a normalizing role, and are consistent with competitive interactions that favor higher-firing neurons, and greater plasticity in lower-firing cells.

# Keywords

Firing-rate homeostasis, REM sleep, non-REM sleep, hippocampus, regression to the mean

## Statement of Significance

To better understand the effects of sleep and awake states on hippocampal neurons with different activity levels, we separated neurons into quantiles based on firing rate and implemented a shuffle correction to account for regression to the mean. During non-REM, REM, and non-REM to REM transitions, low-firing neurons showed either the weakest increase or the largest decrease in firing, whereas at the REM to non-REM transition, low- and high-firing cells respectively increased and decreased their activity. The net effect of sleep was a larger firing decrease in lower-firing neurons, while the net effect of waking was a larger increase in median-firing cells, suggesting greater plasticity among these cells.

# Introduction

Neurons fire to communicate. Rates of firing vary across both time<sup>1,2</sup> and neurons<sup>3,4</sup>. The dynamic range of a neuron's firing is determined by a combination of membrane geometry, distribution and types of ionic conductances, and efficacy of synaptic inputs<sup>5,6</sup>, and can quickly change. Modifications in each of these properties can potentially alter a neuron's gain function or “excitability”. Recent evidence suggests that a neuron’s firing rate is homeostatically regulated<sup>7</sup>, and that modifications in membranes and synapses can work to maintain the neuron's dynamic range<sup>8,9</sup>. Several studies from different labs indicate that these modifications are at least partially state-dependent; the emerging picture is that firing rates of neurons increase during waking<sup>10-12</sup> and decrease during sleep<sup>10,11,13</sup>, in a constant dance around the dynamic range.

Each waking and sleep stage features different levels of neuromodulators, which contribute uniquely to the excitability of neuronal circuits, network firing patterns, and the plasticity of their synapses<sup>14,15</sup>. For example, REM is characterized by high acetylcholine and low noradrenaline, serotonin and histamine levels, while non-REM and waking features intermediate and high levels of these neuromodulators, respectively<sup>14,15</sup>. Unique brainstem and thalamocortical networks are also active within each state, producing state-specific oscillatory firing patterns<sup>15-17</sup>. The differing neuromodulatory and network backgrounds lead to different average firing rates in REM, non-REM, and waking<sup>10,11</sup>, but averaging masks variations within each state. For example, in sequences of non-REM and REM sleep, neuronal firing rates zig-zag, increasing within non-REM and decreasing in REM<sup>10,13</sup>. But while the net effect of these variations is a decrease in firing rate, it is not clear how each of these brain states, at onset and over its duration, affect neurons at different excitability levels. In particular, lower- and higher-firing neurons are presumed to be affected differently by activity-driven homeostasis. Understanding such effects is

further complicated by regression to the mean (RTM), for which the null hypothesis allows that firing rates of low-firing neurons should increase and those of high-firing neurons should decrease. In this report, we aim to investigate changes in firing rates of neurons within different stages of sleep and the effects of transitions between sleep stages, while carefully controlling for RTM.

## Methods

We analyzed data previously recorded from hippocampal CA1 region of four rats. Details of the experimental protocols, including animals, surgery, electrophysiological recoding, spike detection and clustering, and sleep detection can be found in ref (<sup>10</sup>) and are summarized below. All experimental procedures were in accordance with the National Institutes of Health guidelines and approved by the University of Wisconsin-Milwaukee Institutional Animal Care and Use Committee.

**Animals, surgery, and electrophysiological recoding** Four male Long-Evans rats (250 – 350 g; Charles River Laboratories, Wilmington, MA) were implanted with 64-ch silicon probes in the dorsal hippocampus (2.00 mm lateral and 3.36 mm posterior from the bregma) under isoflurane anesthesia. Three were also surgically implanted with two stainless steel wires (AS 636, Cooner wire, Chatsworth, CA) in the nuchal muscles to record electromyography (EMG). After at least 5 days of recovery from the surgery, we recorded local field potentials (LFP) and unit activities continuously for 12 hours in light cycles (9 a.m. – 9 p.m.) and 9 hours in dark cycles (9 p.m. – 6 a.m.), in 19 total sessions. Animals were water-restricted, and ran on a linear track daily from 6 a.m. – 9 a.m. Spike detection and clustering were done, as previously described<sup>10</sup>, on each 9 – 12 hr session separately. Animals were kept in 12-hour light/dark cycles throughout the experiment.

**Sleep detection** Waking and sleep were segregated based on head speed of the rats and amplitudes of the EMG. In an animal that did not have EMG electrodes, we used volume-conducted EMG derived from the brain electrodes instead of nuchal EMG<sup>18, 19</sup>. High theta periods were detected based on the ratio of power in the 5 – 10 Hz band over 1 – 4 Hz and 10 – 14 Hz bands, using a MATLAB script developed by Anton Sirota<sup>20</sup>. High theta during sleep identified REM sleep<sup>21</sup>, and the remaining was non-REM. REM and non-REM epochs < 50 s were excluded from analyses.

**Change index and deflection index** Change index (*CI*) was defined as  $(FR_2 - FR_1)/(FR_2 + FR_1)$ , here  $FR_1$  and  $FR_2$  are firing rates of a neuron. Neuronal population was separated into quintiles based on  $FR_1$  within each epoch, and mean *CI* across epochs was calculated for each quintile. Because neuronal firing rates are log-normally distributed, the difference in logarithm of firing rates,  $\Delta \log(FR)$ , has been used elsewhere to assess firing rate change<sup>18</sup>. Although *CI* and  $\Delta \log(FR)$  generally behave similarly (see supplemental information),  $\Delta \log(FR)$  becomes singular when either  $FR_1$  or  $FR_2$  approach or equal zero. Therefore, in our analysis we opted to use *CI*. In each analysis, we generated 2000 shuffled surrogates by randomly flipping  $FR_1$  and  $FR_2$ , and obtained shuffled mean and 95% confident intervals. The deflection index (*DI*) was defined as difference of *CI* from the surrogate mean.

**Simulation of additive and multiplicative changes.** Starting with  $n = 5000$  “true firing rates” ( $TFR_1$ ) obtained from a log-normal distribution in CA1 pyramidal cells during non-REM sleep ( $0.536 \pm 0.686$  Hz,  $n = 50846$ )<sup>10, 22</sup>, true firing rate in period 2 ( $TFR_2$ ) was determined based on:

$$\text{For no change: } TFR_2 = TFR_1$$

$$\text{For multiplicative decrease: } TFR_2 = (1 - a) \times TFR_1$$

$$\text{For subtractive decrease: } TFR_2 = TFR_1 - b.$$

For our example, we set  $a = 0.090$  and  $b = 0.052$ , to match the mean ratio and difference between non-REM epochs in non-REM<sub>*i*</sub>/REM/nonREM<sub>*i+1*</sub> triplets.

We also considered additive noise ( $SD_a$ ) and multiplicative noise ( $SD_m$ ) estimated from these triplets:

$$SD_a = \sqrt{2} \cdot RMS\left(\frac{FR_{i,j} - FR_{i+1,j}}{2}\right),$$

$$SD_m = \sqrt{2} \cdot RMS\left(\frac{FR_{i,j} - FR_{i+1,j}}{(FR_{i,j} + FR_{i+1,j})/2}\right),$$

where  $FR_{i,j}$  is the firing rate of cell  $j$  in period  $i$ , and  $RMS(\bullet)$  is root mean square across all cells in all triplets ( $n=15555$ ). Our example (Figure 1) was generated by inducing additive or multiplicative noise as follows ( $n=1,2$ ):

$$\text{for additive noise: } FR_n = TFR_n + N_a,$$

$$\text{for multiplicative noise: } FR_n = TFR_n \times (1 + N_m),$$

where  $N_a$  and  $N_m$  were zero-mean Gaussian distributed random values whose SDs,  $SD_a$  and  $SD_m$ , were determined above ( $SD_a = 0.171$ ,  $SD_m = 0.592$ ).

## Results

We first set out to understand the relationship between variability and RTM in a population of neurons with log-normally distributed firing rates. We reasoned that variability might be either “additive noise”, affecting all neurons by an equal amount, or else “multiplicative noise”, proportional to each neuron’s firing rate (also see Methods). These scenarios are depicted for two snapshots from a population of neurons ( $n = 5000$ ) where the only change comes from the noise term (Figure 1A). Naturally, additive noise has a larger relative effect on low-firing neurons.

However, under both scenarios, lower-firing neurons show an apparent increased firing, while higher-firing neurons show an apparent decreased firing. This is RTM and can confound evaluations of true effects (e.g. from sleep). To control for this RTM, we instated a shuffling method in which we randomly flipped before/after indices and repeated the analysis multiple times to obtain a surrogate distribution. Under either (additive/multiplicative) noise scenario this surrogate data provided us with valuable “control” shuffle means and confidence intervals for each quintile. We defined the “deflection index (*DI*)” as the difference between the observed change index (*CI*) and the surrogate mean within each quintile. These *DI*s were not significantly different from zero when changes were due only to noise (Figure 1A).

We then examined *DI*s under two scenarios with a simulated effect in addition to noise: when firing rates were decreased across the population, either multiplicatively (Scenario 1), by an amount proportional to each cell’s initial firing rate, or additively (Scenario 2), by a fixed amount for all cells (Figure 1B, C). Parameters for these effects were chosen to simulate real data across non-REM sleep (see Methods). In both scenarios, despite the incorporated decrease, lower-firing neurons appeared to increase firing, based on the *CI*s. However, under Scenario 1 the evaluated *DI*s correctly depicted a uniform decrease across the population (Figure 1B). Meanwhile the additive decrease under Scenario 2 produced a larger relative effect on the *DI* in low-firing cells than in high-firing cells (Figure 1C), as expected. Thus, the shuffle-method produces *DI*s that can effectively describe and differentiate the two scenarios under either noise model, and control for RTM.

We next applied this method to hippocampal firing changes within non-REM and REM stages of sleep. During non-REM sleep, the average firing rates of (putative) pyramidal neurons increased ( $CI = 0.058 \pm 0.002$ ,  $p < 10^{-300}$ , Wilcoxon signed-rank test; Figure 2A). While the *CI*



alone appears to show the largest increase in low-firing cells, and a decrease in the highest-firing quintile, when shuffle corrected, in fact all quintiles, as well as (putative) interneurons, showed a firing-rate increase (Figure 2A). While lower-firing cells appeared to show a smaller relative increase, firing increases were more uniform when we separated epochs depending on time-of-day and sleep-history (Figure S1 A-C). During REM sleep, we found an overall net decrease ( $CI = -0.030 \pm 0.003$ ,  $p = 5.4 \times 10^{-19}$ , Wilcoxon signed-rank test; Figure 2B), including in interneurons. This decrease was apparently additive: lower-firing cells showed the largest relative firing decreases over the course of a REM sleep epoch. The magnitude and significance of this decrease was, however, dependent on time-of-day and subsequent sleep/wake state (Figure S1 D&E). These changes did not appear to reflect a change in the balance between excitation and inhibition within either non-REM or REM states<sup>23</sup>.

While firing rates of neurons change within each sleep stage, they also change between different stages. How a change in neuromodulatory background between sleep stages affects lower- and higher-firing neurons has not explicitly been tested. We therefore compared firing-rate quintiles across transitions from the last third of non-REM to the first third of the subsequent REM epochs, and from the last third of REM to the first third of the subsequent non-REM epochs. Non-REM to REM transitions were marked by an overall decrease ( $CI = -0.186 \pm 0.003$ ,  $p < 10^{-300}$ , Wilcoxon signed-rank test; Figure 2C), with decreased firing in lower-firing cells but increased firing in higher-firing cells. Interneuron firing also increased, potentially driving some of the differences. In contrast, when REM transitioned to non-REM sleep, lower-firing quintiles showed increased firing while higher-firing quintiles and interneurons showed a firing decrease (Figure 2D). Interestingly, this transition was the only one we investigated that was not comparatively dominated by higher-firing neurons, but was instead marked by a renormalizing

effect on firing rates across quintiles. Thus, non-REM sleep was unique in providing the initial background state for the most uniform firing among the population of cells, potentially because of lower effective inhibition.

The transition patterns were remarkably stable across early and late sleep in both light and dark cycles (not shown). However, the within-state changes during non-REM and REM sleep somewhat varied according to time-of-day and preceding/following states (Figure S1). Quintiles in non-REM sleep following waking in early light-cycle sleep (9 a.m. – 3. p.m.) did not show the otherwise typical firing increases (Figure S1), likely because firing rates were saturated following awake track running (6 a.m. – 9 a.m.)<sup>10</sup>; these patterns resumed shortly thereafter following REM sleep. It may be worth noting that this first non-REM sleep following behavior (often called “post-sleep”) is in fact the most widely investigated epoch across the circadian cycle<sup>24, 25</sup>, though it is the most anomalous. Additionally, in non-REM epochs that transitioned to waking, firing rates in fact decreased during the light cycle (when rats sleep most), but increased in the dark cycle. For REM sleep preceding non-REM, decreased firing was also observed mainly in the early light cycle (9 a.m. – 3. p.m.), while in REM before waking, a large decrease was seen in the late dark cycle (1:30 a.m. – 6 a.m.).

A recent study reported differential firing rate changes among low- and high-firing prefrontal cortical cells across microarousals, with waking EMG levels, during non-REM sleep<sup>18</sup>. We did not observe such microarousals in our recordings. However, we did observe extended (~ 5s) periods of low-amplitude sleep, within non-REM, marked by substantially decreased power in the hippocampal local field potential and cortical EEG < 50 Hz<sup>26</sup>. We refer to these as LOW states. LOW states may share features with microarousals<sup>18, 27, 28</sup>, but were much shorter (~ 5s compared to ~ 16s) and were not accompanied by increased EMG<sup>26</sup>. We then examined how

LOW states affect hippocampal firing patterns<sup>18</sup>. Comparing firing rates in non-REM from before (pre-) to after (post-) LOW states (Figure 3A), the *CI* indicated increased firing in low-firing cells and decreased firing in high-firing cells, as reported for prefrontal neurons before and after microarousals<sup>18</sup>. However, when we corrected for RTM, the firing increase actually occurred in higher-firing neurons, and lower-firing neurons decreased firing. Similarly, when we investigated firing changes across consecutive LOW states, within non-REM sleep (Figure 3B), low-firing and high-firing neurons respectively appeared to increase and decrease firing, but this pattern reversed in the *DI*, shuffle corrected for RTM. These observations highlight the importance of correcting for RTM and suggest that LOW states differential affect firing in lower and higher-firing cells.

To summarize and compare the effects we have observed for REM and non-REM sleep along with waking and the net result across sleep, we plotted changes in quintiles (and for interneurons) on the same scale (Figure 4). This fixed scale well demonstrates that the largest changes occurred between, rather than within states and, aside from the REM to non-REM sleep transition, most changes were anti-normalizing. It also illustrates the comparative effects of transitions between waking and sleep. Within waking, firing rates increased ( $CI = 0.111 \pm 0.010$ ,  $p = 1.9 \times 10^{-27}$ , Wilcoxon signed-rank test; Figure S3F) and preferentially in median-firing neurons<sup>10</sup>. Falling asleep was marked by an increase in firing rates in all quintiles ( $CI = 0.254 \pm 0.004$ ,  $p < 10^{-300}$ , Wilcoxon signed-rank test; Figure S3G), but with the largest increase in the median quintile. On the other hand, waking up from either non-REM (Figure S3D) or REM sleep (Figure S3E) was marked by a relatively larger decrease in low-firing neurons, which were again the quintile most readily changed. To evaluate how net hippocampal firing changed across entire sequences of non-REM/REM sleep (bottom, Figure 4), we compared the first third of non-REM<sub>i</sub>

to the first third of the subsequent non-REM<sub>i+1</sub> epoch (Figure S3A). Consistent with our previous report<sup>10</sup>, we found that, overall, firing decreased in all quintiles, but with a larger effect in lower than in higher-firing neurons. Likewise, across longer extended sequences of non-REM and REM sleep (> 30 min without interruption > 60 sec), firing rates of lower-firing cells decreased more (Figure S3C). Interneuron firing decreased as well, illustrating that this firing decrease was not due to a rebalance in excitation and inhibition. Somewhat surprisingly, we did not observe similar changes when comparing the first third of REM<sub>i</sub> to the first third of the subsequent REM<sub>i+1</sub> epoch (Figure S3B). This may be because of greater firing variability or saturated firing during REM sleep<sup>10</sup> that masks changes across sleep. However, this change was also manifest when we compared the last minute of waking before to the first minute of waking after extended sleep sequences (Figure S3C), with, again, a greater decrease seen in lower-firing cells. We also considered the possibility that each neuron has its own set point within the log-normal range of firing rates, and that sleep and waking move neurons relative to their individual set points<sup>7</sup>. For this analysis, rather than investigating changes across firing rates, we calculated ratio of firing rate for each neuron relative to their session mean firing rates (Figure S3) and determined quantiles by combining all epochs. Interestingly, these patterns were highly similar to those seen in Figure 4 without individual normalization.

## Discussion

In this work, we aimed to understand how lower and higher firing neurons were affected during and across REM and non-REM sleep and waking states, which is important for a better understanding of the function(s) of sleep states in mammals. We tested for RTM under two conditions. In the presence of multiplicative noise, lower-firing cells showed an apparent firing increase while higher-firing neurons showed a similar apparent decrease. When noise was

additive, lower-firing cells showed a relatively larger effect. Some combination of additive and multiplicative variability is likely to be present in neuronal recordings. Overall, this analysis advocates caution in interpretation of increases and decreases that affect lower and higher firing neurons respectively. RTM alone describes a basic homeostatic effect. By measuring changes relative to a surrogate distribution obtained by random shuffles of the real data, we were able to measure effects beyond RTM, with significance determined by effect size and variability in the data. We found that, in general, sleep states and state transitions do not affect neurons uniformly, but that the changes depend on the relative excitability of cells, which likely reflect a combination of neuromodulation of membrane excitability<sup>29</sup>, sleep-dependent network dynamics<sup>23, 30</sup>, and synaptic input to the respective cells<sup>31-33</sup>.

Most of the states and transitions we investigated and their net effects favored (increased or maintained) high-firing cells over low-firing ones. Interestingly, the transition from REM to Non-REM was the only timepoint that we saw a simultaneous increase in lower-firing cells and a decrease in higher-firing ones, which served to partially renormalize firing across the population. Such an equitable effect was also present when we evaluated each neuron's firing relative to its own session mean. Thus, upon transition from REM to non-REM, cells firing below their mean rates, increased firing while those firing above their means tended to decrease. Perhaps non-REM sleep, relatively devoid of neuromodulation and external sensory influence, provides the most equitable brain state for neurons. But as a non-REM epoch develops, neuronal firing rates increase<sup>10, 13</sup>. The shuffle-corrected firing increases were significant across quantiles, though exact patterns depended on time-of-day and preceding/following states, (Figure S1). Likewise, during REM sleep, shuffle-corrected firing rates decreased across the population, and with a

lower decrease in higher-firing neurons. More dramatically, the non-REM to REM transition lead to a firing increase in the higher-firing cells, but a decrease in lower-firing cells.

There may be several explanations for these observations. One possibility is that during most of sleep, except non-REM, there is competition between assemblies of neurons, with the winner determined by the assemblies starting with a higher-firing advantage. Such a winner-take-all mechanism may be implemented in a recurrently connected circuit along with inhibition<sup>34-36</sup>, such as region CA3, one synapse upstream from our CA1 recordings. Consistent with this conjecture, interneuron firing rates were at their lowest during non-REM sleep<sup>10</sup>, potentially signifying a shift in the balance of excitation and inhibition towards normalized firing rates, and away from winner-take-all. A second possibility, compatible with the first, is that sleep is composed of multiplicative changes in firing rates coupled with additive decreases. These decreases therefore affect all neurons by a similar amount, regardless of whether they are high or low firing cells, and they are manifest by a higher-relative decrease in lower-firing neurons.

The net effects of these transitions, from the beginning of one non-REM epoch to the beginning of the next one, or from the end of waking to its subsequent onset, were consistent with previous reports<sup>10, 18</sup>: firing rates decreased in all quantile over sleep, but preferentially in lower-firing neurons. Whereas large state and state-transition effects are likely attributed to the combination of excitability effects discussed above, we and others have conjectured that the slower firing rate decreases over sleep are indeed produced by synaptic downscaling<sup>10, 11, 13, 37</sup>. If this conjecture is correct, the greater relative decrease in lower-firing neurons may be indicative of an additive decrease, in which all synapses are downscaled by the same amount, which would have the effect of improving signal-to-noise in higher firing cells. The final result appears tantamount to greater plasticity in the synapses of lower-firing than higher-firing neurons<sup>18, 38</sup>.

## Figure legends

### Figure 1

**Simulated noise and firing decreases affect low- and high firing cells differently.** Log-normally distributed firing rates ( $n = 5000$ ) were simulated (see Methods) with additive noise ( $\text{Noise}_{\text{add}}$ , left columns) and multiplicative noise ( $\text{Noise}_{\text{mult}}$ , right columns). Top panels show density plots of firing rate with identity (white lines). Black crosses indicate means of  $FR_1$  and  $FR_2$ . Cells were separated into quintiles based on  $FR_1$ . Change indices ( $CI$ , middle panels) and deflection indices ( $DI$ , bottom panels) were calculated for each quintile. Gray bands show 95% confidence intervals obtained from surrogate (shuffle) distributions. (A) Because of regression to the mean, with noise alone, low- and high-firing quintiles had positive and negative  $CI$ s, respectively. However, shuffle-corrected  $DI$ s were not significantly different from zero. (B) With a multiplicative decrease,  $CI$ s showed similar patterns to noise (A), but  $DI$ s demonstrated a uniform decrease across quintiles. (C) In contrast, an additive decrease had a greater relative effect on lower-firing cells. Error bars indicate SEM.

### Figure 2

**Firing rate changes within sleep states and upon transitions between sleep states.** Density plot of firing rates (top panels) with identity lines (white) and means (black crosses). Change indices ( $CI$ , middle panel) and deflection indices ( $DI$ , bottom panels) are shown for each quintile along with 95% confidence intervals (gray bands), as well as for interneurons. (A) Within non-REM (50846 pyramidal cells and 5694 interneurons in 925 epochs), firing rates increased across quintiles, with a greater increase in higher-firing neurons, not apparent in  $CI$ s. (B) Within REM (24113 pyramidal cells and 2782 interneurons in 456 epochs), an apparent additive decrease was

observed, showing a greater decrease in low-firing quintiles. (C) Upon transition from non-REM to REM (21832 pyramidal cells and 2523 interneurons in 405 transitions), an anti-normalizing change was observed: lower-firing cells decreased firing but high-firing cells increased firing. (D) In contrast, a normalizing change was observed upon transition from REM to non-REM (17385 pyramidal cells and 1989 interneurons in 326 transitions). Error bars indicate SEM, \*\*\*  $p < 0.001$ .

### Figure 3

**Firing rate changes across LOW amplitude sleep within non-REM epochs.** Density plots of firing rates (top panels), change indices ( $CI$ , middle panels), and deflection indices ( $DI$ ; bottom panels) were calculated between non-REM (NREM) periods before and after LOW amplitude sleep (A; 416895 cells in 10128 sequences)<sup>26</sup>. In (B), consecutive LOW states, separated by non-REM, are compared (B; 158084 cells in 11439 sequences). \*  $p < 0.05$ , \*\*\*  $p < 0.001$ .

### Figure 4

**Firing rate changes across sleep.** Summary plot of changing deflection indices through multiple non-REM (NREM) and REM epochs (see also Figure S2) shown on the same scale. Top panels depict average changes within epochs (note also Figure S1: these can vary depending on time-of-day and preceding/following states), and upon transitions. Bottom panels show changes from the first third of NREM<sub>*i*</sub> (or REM<sub>*i*</sub>) to the first third of NREM<sub>*i+1*</sub> (or REM<sub>*i+1*</sub>) for all quintiles, as well as changes from the last minute of waking before sleep (Wake<sub>*i*</sub>) to the first minute of waking after sleep (Wake<sub>*i+1*</sub>). Error bars indicate SEM.



## Supplemental Information

**Change index and difference in log firing rate.** Because neuronal firing rates are log-normally distributed, a recent study used the difference of log firing rates ( $\Delta \log FR$ ) to evaluate firing changes across sleep<sup>18</sup>. We therefore compared this measure to the  $CI$  we use here and elsewhere<sup>10</sup>. When firing rates  $FR_i = TFR + N$  ( $i = 1, 2$ ), (true firing rate plus noise)  $\Delta \log FR$  and  $CI$  are given as follows:

$$\Delta \log FR = \log(FR_2) - \log(FR_1) = \log\left(1 + \frac{2N}{TRF - N}\right),$$

$$CI = \frac{FR_2 - FR_1}{FR_2 + FR_1} = \frac{N}{TRF}$$

Thus,  $\Delta \log FR$  and  $CI$  are related by:

$$\Delta \log FR = \log\left(1 + \frac{2CI}{1 - CI}\right)$$

When  $N \ll TRF$ ,  $\Delta \log FR \sim 2CI$ . However, when  $N \rightarrow TRF$  (and/or  $FR_i \rightarrow 0$ ), unlike  $CI$ ,  $\Delta \log FR$  diverges. We therefore prefer to employ the  $CI$  to evaluate changes.

## Supplemental Figure Legends

### Figure S1

**Changes within non-REM are affected by the timing and history of sleep.** Deflection indices ( $DI$ ) were calculated within non-REM epochs that followed waking (A), interleaved REM (B) or preceded waking (C) in early light (9 a.m. – 3 p.m.; top row), late light (3 p.m. – 9 p.m.; second row), early dark (9 p.m. – 1:30 a.m.; third row) and late dark (1:30 a.m. – 6 a.m.; bottom row) periods, separately. In light cycles, firing rate did not further increase during non-REM following waking (A), likely because of saturated firing. Firing rate robustly and uniformly increased in

non-REM interleaving REM (B). Unlike at other times, in non-REM preceding awake in light cycles (C), firing rates actually decreased. In REM preceding non-REM (D), firing decreases, affecting low-firing cells most strongly, were mainly seen in early light. In REM preceding waking (E), firing decreases were seen mainly in the late dark cycle. The number of analyzed cells are shown at top right corner in each plot (black for pyramidal cells, gray for interneurons).

\*  $p < 0.05$ , \*\*  $p < 0.01$ , \*\*\*  $p < 0.001$ . Error bars indicate SEM.

## Figure S2

**Firing rate changes at state transitions.** Density plots of firing rates (top) with identity lines (white) and means (cross), change indices ( $CI$ ; middle) and deflection index ( $DI$ ; bottom) in each quintile of pyramidal cells are shown, along with interneurons. Gray bands indicates surrogate mean and 95% confidence intervals. The comparisons are as follows: (A) first and last minutes of stable waking (1775 pyramidal cells and 54 interneurons in 46 stable wake), (B) state transitions from last minute of awake to first third of non-REM (NREM; 14494 pyramidal cells and 1508 interneurons in 251 transitions). (C) transitions from last third of non-REM to first minute of awake (12049 pyramidal cells and 1372 interneurons cells in 214 transitions), (D) transitions from last third of REM to first minute of awake (1802 pyramidal cells and 241 interneurons in 32 transitions), (E) between the first third of non-REM epochs in non-REM<sub>*i*</sub>/REM/non-REM<sub>*i+1*</sub> triplets (15555 pyramidal cells and 1778 interneurons in 288 triplets), (F) last and first one minutes of awake separated by sleep (3800 pyramidal cells and 704 interneurons in 99 sleep), (G) first third of REM epochs in REM<sub>*i*</sub>/non-REM/REM<sub>*i+1*</sub> triplets (8690 pyramidal cells and 1051 interneurons cells in 167 triplets).

## Figure S3

**Summary of changes in normalized firing rates.** Firing rates were normalized by the ratio of each neuron's firing rate to its session mean, pooled across epochs, then separated into quintiles. The same shuffling method as before was used to generate surrogates. Patterns were remarkably similar to those for log-normal (non-normalized) firing rates (Figure 4). Error bars indicate SEM.

## References

1. Rieke F. Spikes : exploring the neural code. Cambridge, Mass.: MIT Press, 1997.
2. Amarasingham A, Chen TL, Geman S, Harrison MT, Sheinberg DL. Spike count reliability and the Poisson hypothesis. *J Neurosci* 2006;26:801-9.
3. Roxin A, Brunel N, Hansel D, Mongillo G, van Vreeswijk C. On the distribution of firing rates in networks of cortical neurons. *J Neurosci* 2011;31:16217-26.
4. Buzsaki G, Mizuseki K. The log-dynamic brain: how skewed distributions affect network operations. *Nat Rev Neurosci* 2014;15:264-78.
5. Koch C. Biophysics of computation : information processing in single neurons. New York: Oxford University Press, 1999.
6. Stuart GJ, Spruston N. Dendritic integration: 60 years of progress. *Nat Neurosci* 2015;18:1713-21.
7. Hengen KB, Lambo ME, Van Hooser SD, Katz DB, Turrigiano GG. Firing rate homeostasis in visual cortex of freely behaving rodents. *Neuron* 2013;80:335-42.
8. Turrigiano G. Too many cooks? Intrinsic and synaptic homeostatic mechanisms in cortical circuit refinement. *Annu Rev Neurosci* 2011;34:89-103.
9. Marder E, Goaillard JM. Variability, compensation and homeostasis in neuron and network function. *Nat Rev Neurosci* 2006;7:563-74.
10. Miyawaki H, Diba K. Regulation of Hippocampal Firing by Network Oscillations during Sleep. *Curr Biol* 2016;26:893-902.
11. Vyazovskiy VV, Olcese U, Lazimy YM, et al. Cortical firing and sleep homeostasis. *Neuron* 2009;63:865-78.
12. Hengen KB, Torrado Pacheco A, McGregor JN, Van Hooser SD, Turrigiano GG. Neuronal Firing Rate Homeostasis Is Inhibited by Sleep and Promoted by Wake. *Cell* 2016;165:180-91.
13. Grosmark AD, Mizuseki K, Pastalkova E, Diba K, Buzsaki G. REM sleep reorganizes hippocampal excitability. *Neuron* 2012;75:1001-7.
14. Hobson JA, Pace-Schott EF. The cognitive neuroscience of sleep: neuronal systems, consciousness and learning. *Nat Rev Neurosci* 2002;3:679-93.
15. Brown RE, Basheer R, McKenna JT, Strecker RE, McCarley RW. Control of sleep and wakefulness. *Physiol Rev* 2012;92:1087-187.
16. Saper CB, Fuller PM, Pedersen NP, Lu J, Scammell TE. Sleep state switching. *Neuron* 2010;68:1023-42.
17. Lee SH, Dan Y. Neuromodulation of brain states. *Neuron* 2012;76:209-22.

18. Watson BO, Levenstein D, Greene JP, Gelinas JN, Buzsaki G. Network Homeostasis and State Dynamics of Neocortical Sleep. *Neuron* 2016;90:839-52.
19. Schomburg EW, Fernandez-Ruiz A, Mizuseki K, et al. Theta phase segregation of input-specific gamma patterns in entorhinal-hippocampal networks. *Neuron* 2014;84:470-85.
20. Sirota A, Montgomery S, Fujisawa S, Isomura Y, Zugaro M, Buzsaki G. Entrainment of neocortical neurons and gamma oscillations by the hippocampal theta rhythm. *Neuron* 2008;60:683-97.
21. Robinson TE, Kramis RC, Vanderwolf CH. Two types of cerebral activation during active sleep: relations to behavior. *Brain Res* 1977;124:544-9.
22. Mizuseki K, Buzsaki G. Preconfigured, skewed distribution of firing rates in the hippocampus and entorhinal cortex. *Cell Rep* 2013;4:1010-21.
23. Dehghani N, Peyrache A, Telenczuk B, et al. Dynamic Balance of Excitation and Inhibition in Human and Monkey Neocortex. *Sci Rep* 2016;6:23176.
24. Rasch B, Born J. About sleep's role in memory. *Physiol Rev* 2013;93:681-766.
25. Genzel L, Kroes MC, Dresler M, Battaglia FP. Light sleep versus slow wave sleep in memory consolidation: a question of global versus local processes? *Trends Neurosci* 2014;37:10-9.
26. Miyawaki H, Billeh YN, Diba K. Low activity microstates during sleep. *bioRxiv* 2016.
27. Halasz P. Hierarchy of micro-arousals and the microstructure of sleep. *Neurophysiol Clin* 1998;28:461-75.
28. Jarosiewicz B, Skaggs WE. Level of arousal during the small irregular activity state in the rat hippocampal EEG. *J Neurophysiol* 2004;91:2649-57.
29. Nadim F, Bucher D. Neuromodulation of neurons and synapses. *Curr Opin Neurobiol* 2014;29:48-56.
30. Peyrache A, Dehghani N, Eskandar EN, et al. Spatiotemporal dynamics of neocortical excitation and inhibition during human sleep. *Proc Natl Acad Sci U S A* 2012;109:1731-6.
31. Timofeev I, Grenier F, Steriade M. Impact of intrinsic properties and synaptic factors on the activity of neocortical networks in vivo. *J Physiol Paris* 2000;94:343-55.
32. Steriade M, Timofeev I, Grenier F. Natural waking and sleep states: a view from inside neocortical neurons. *J Neurophysiol* 2001;85:1969-85.
33. Harris KD, Thiele A. Cortical state and attention. *Nat Rev Neurosci* 2011;12:509-23.
34. Yuille AL, Geiger D. Winner-take-all mechanisms. In: Arbib MA, ed. *Handbook of Brain Theory and Neural Networks*: Mit Press, 1995:1--1056.
35. Lee DK, Itti L, Koch C, Braun J. Attention activates winner-take-all competition among visual filters. *Nat Neurosci* 1999;2:375-81.
36. Rutishauser U, Douglas RJ, Slotine JJ. Collective stability of networks of winner-take-all circuits. *Neural Comput* 2011;23:735-73.
37. Tononi G, Cirelli C. Sleep and the price of plasticity: from synaptic and cellular homeostasis to memory consolidation and integration. *Neuron* 2014;81:12-34.
38. Grosmark AD, Buzsaki G. Diversity in neural firing dynamics supports both rigid and learned hippocampal sequences. *Science* 2016;351:1440-3.

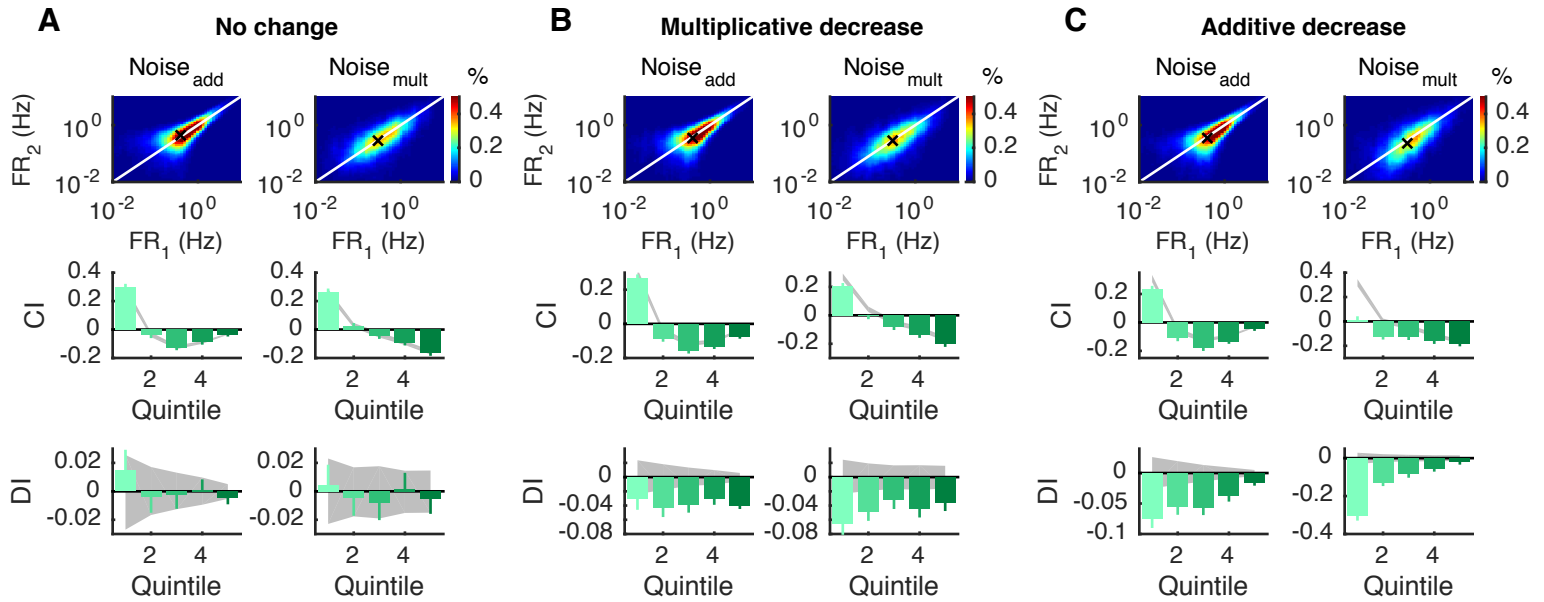


Figure 1

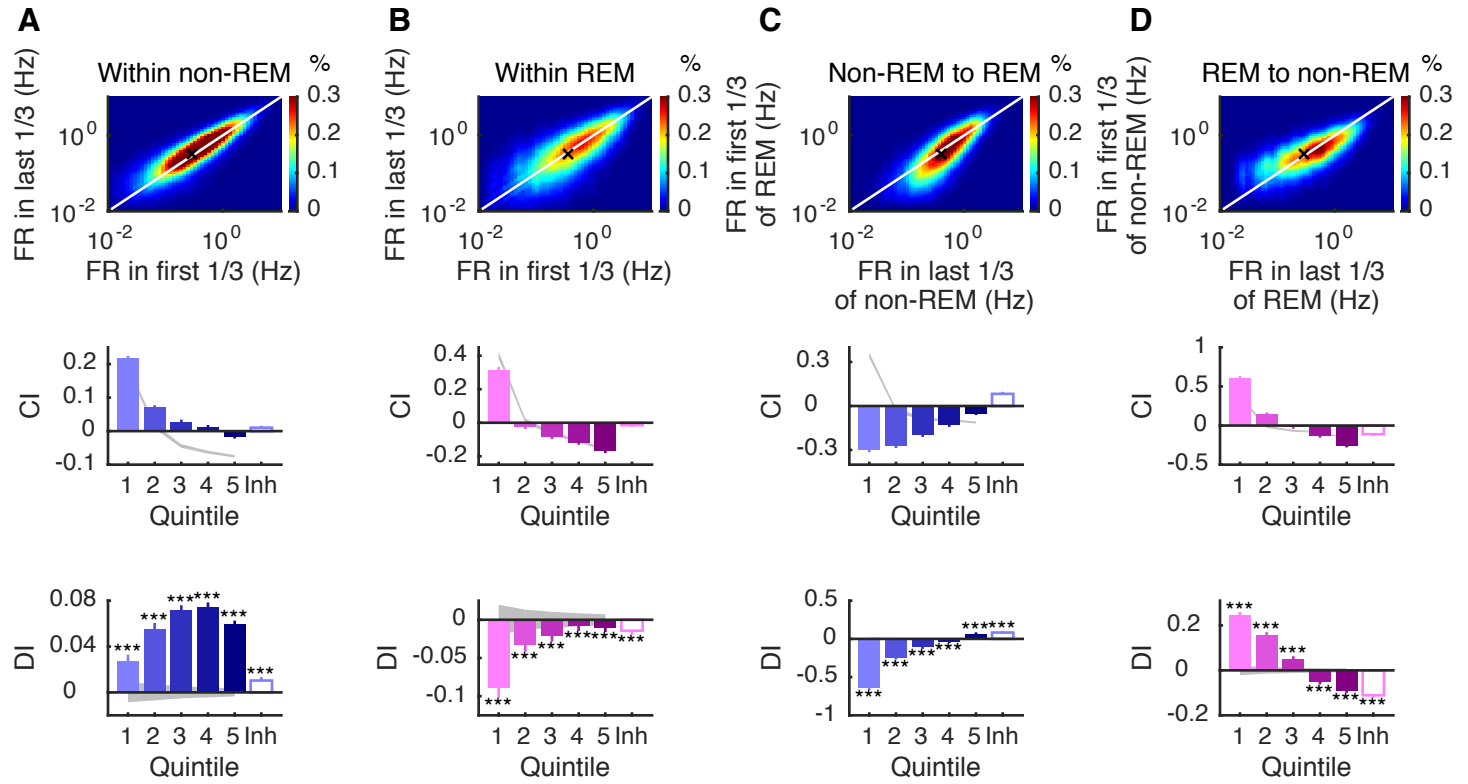
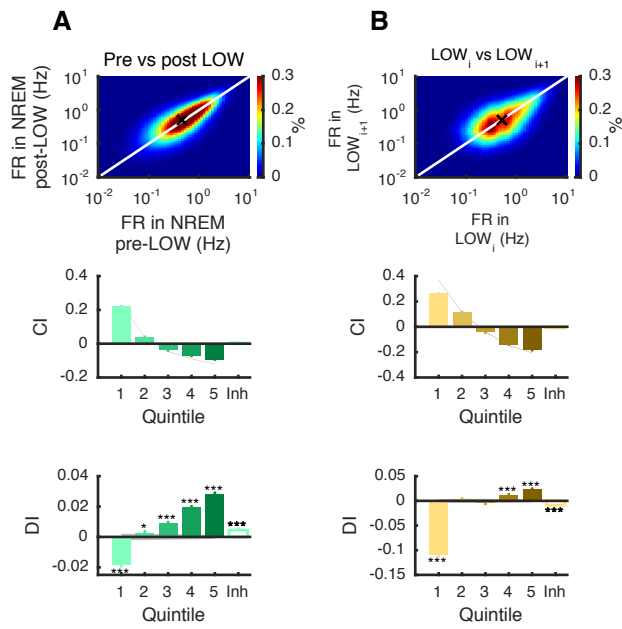


Figure 2



**Figure 3**

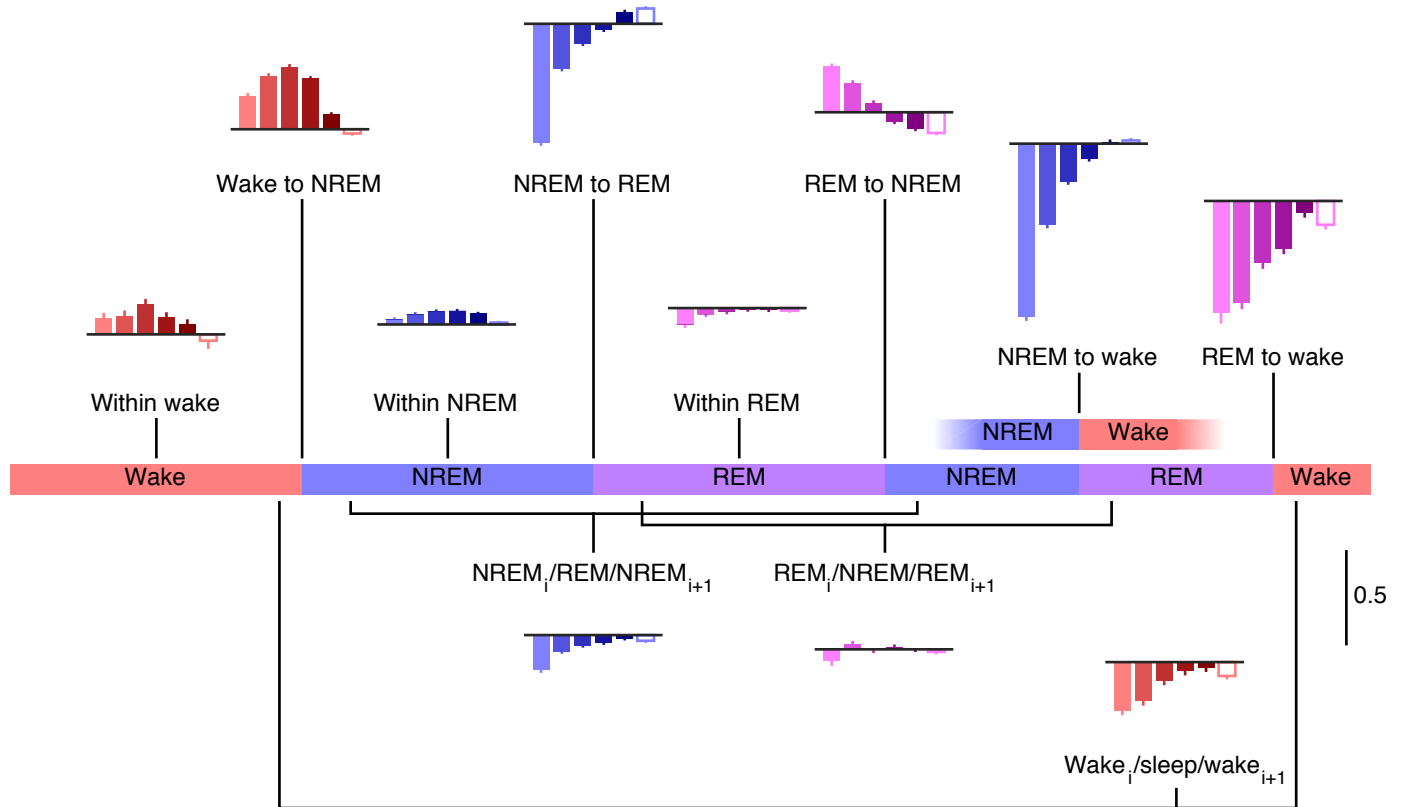
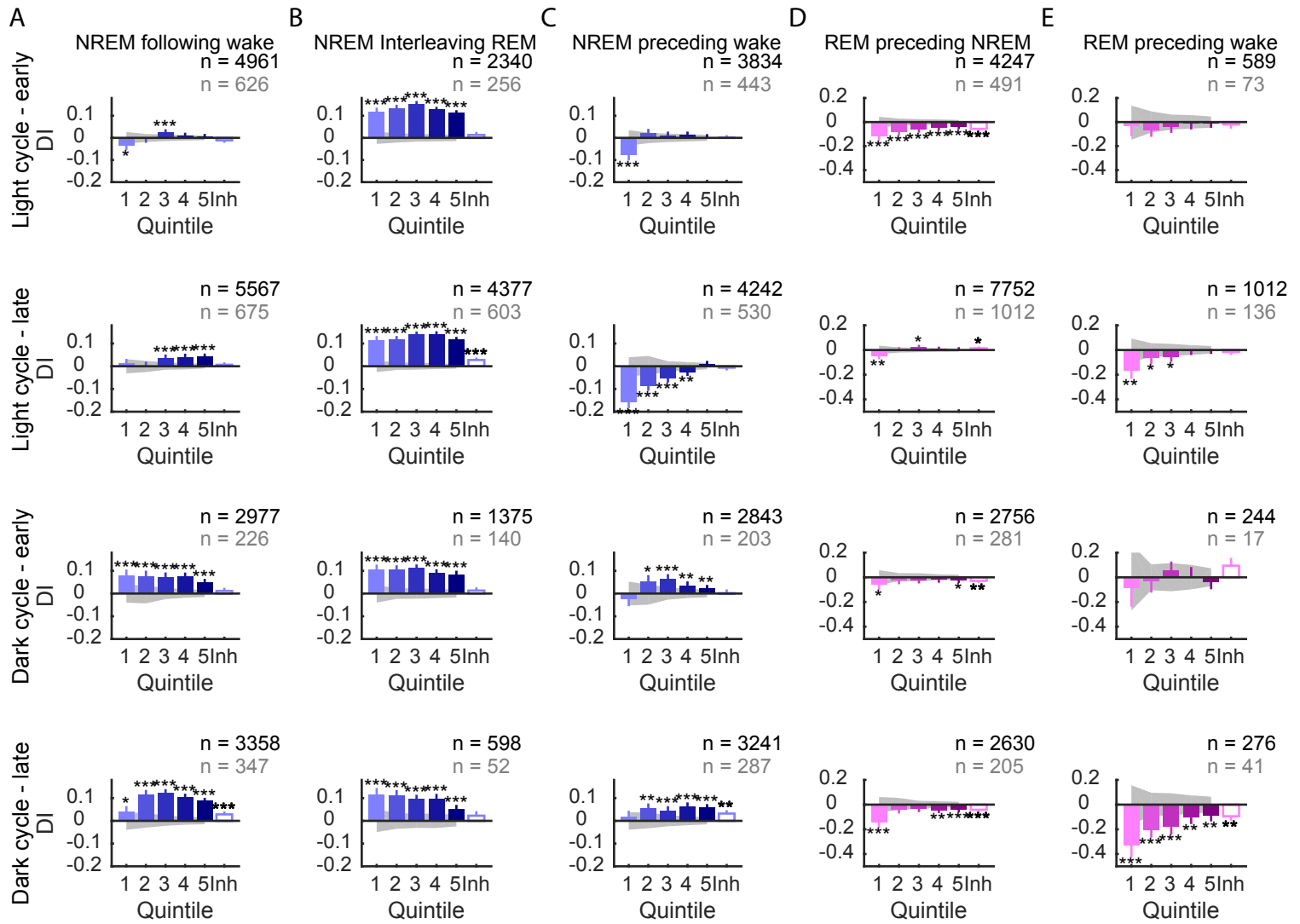


Figure 4





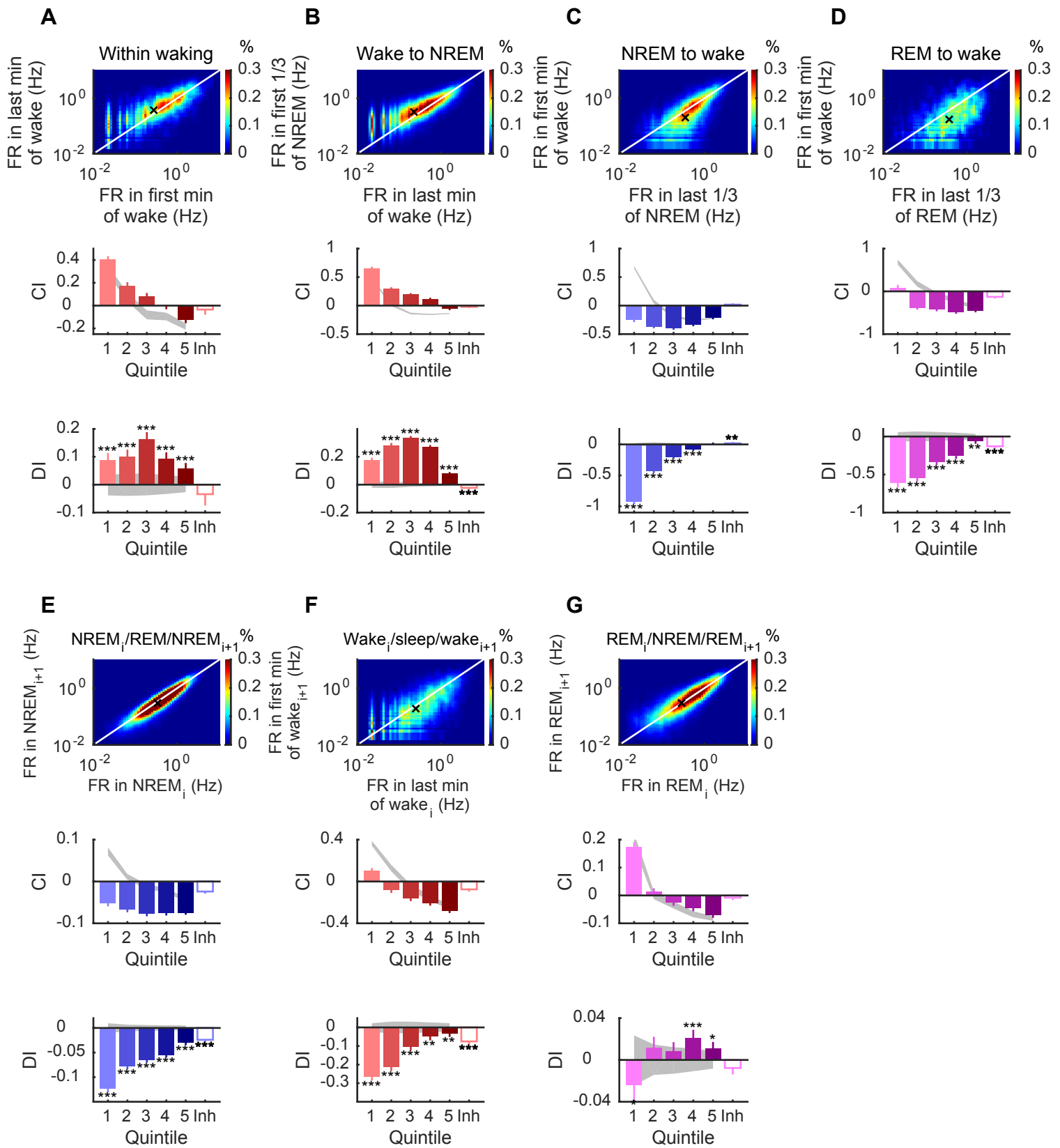


Figure S2

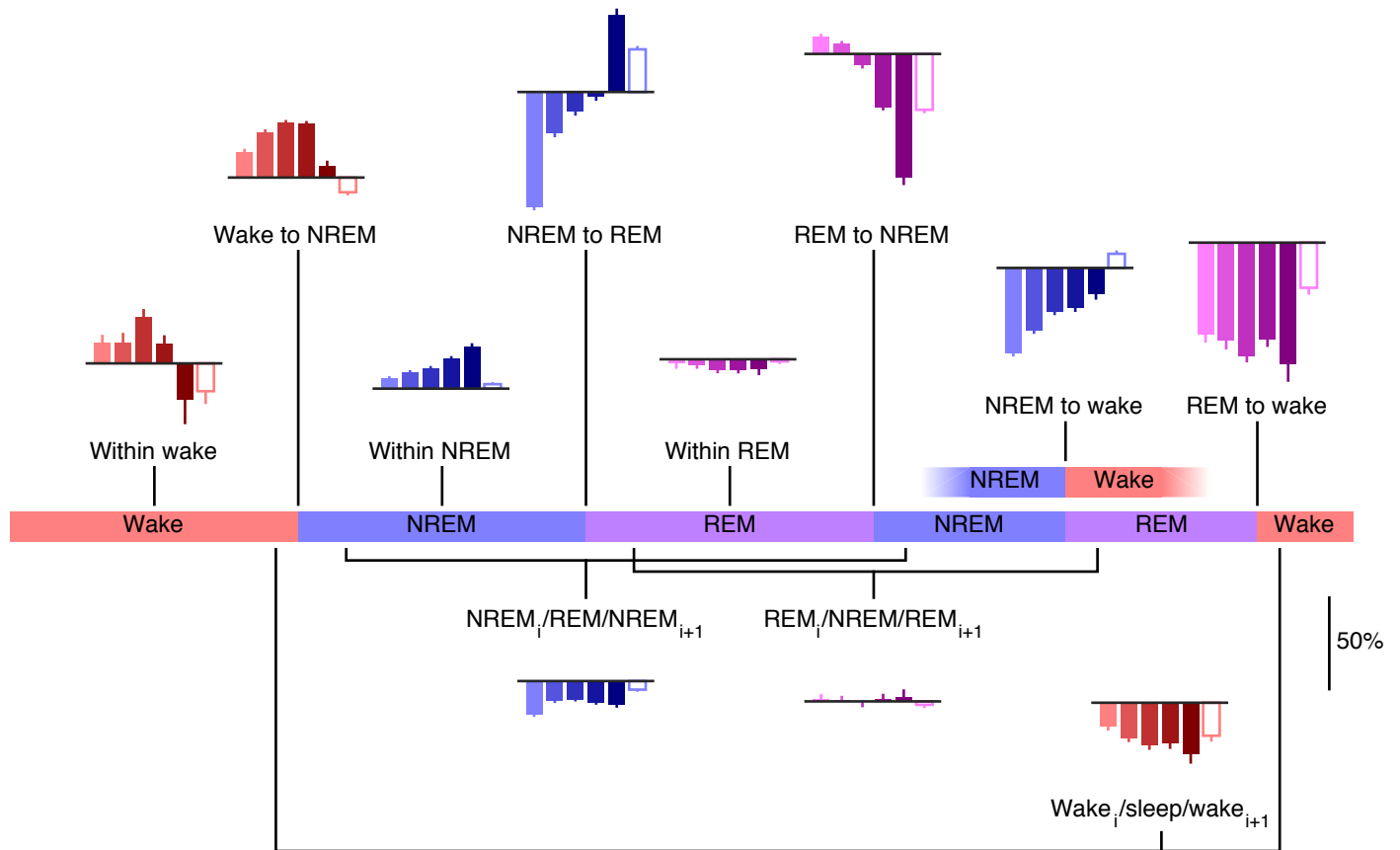


Figure S3